Semiclassical study of spectral evolution under propagation in an active medium

L. You
Institute for Theoretical Atomic and Molecular Physics, Harvard-Smithsonian Center for Astrophysics, 60 Garden Street, MS 14, Cambridge, Massachusetts 02138

J. Cooper
Joint Institute for Laboratory Astrophysics, University of Colorado and National Institute of Standards and Technology, Boulder, Colorado 80309-0440
(Received 7 September 1994)

We study the propagation of a near-resonant strong laser light with a broad background continuum spectrum in a dense gaseous two-level medium. Due to the nonlinear saturation caused by the driving of the coherent component of the field, spectral regions close to the Rabi sidebands with significant gain exist close to the resonance. The subsequent evolution of the spectrum of the propagating field displays interesting features, and in the stationary limit a broadening of the spectral line always eventually happens in the end which contradicts the coherent narrowing phenomenon for pulsed propagation. This may shed some new light on the mechanisms of cone emission.

PACS number(s): 42.50.−p, 03.65.−w, 32.80.−t

I. INTRODUCTION

In many studies of light-matter interaction involving propagation, semiclassical Maxwell-Bloch equations are used quite successfully [1–6], even though, as a mean field theory, they do not describe fully quantum fluctuations [7–13]. When quantum noise is involved in the problem, it is usually difficult to determine the validity for the semiclassical approximation. In most cases, an initiation process involving the generation of new frequency components of light close to the Rabi sidebands exists [7–13]. The generation process depends critically on the properties of quantum noise.

Here we report a semiclassical study of the propagation of a near-resonant strong laser light with a broad background continuum spectrum in a dense gaseous two-level medium [11–13]. The aim of this study was originally to try to understand the validity of a linearization approximation used when studying the propagation of a classical saturating coherent monochromatic field together with two weak symmetrically displaced sidebands of frequencies close to the Rabi sidebands. This linearization approximation is equivalent to assuming that the sidebands are well represented by coherent fields [14–17]. A broad background is used in this paper to simulate generation of the sidebands by amplified spontaneous emission (ASE), whereas the usual model examines the propagation with weak coherent sidebands. The usual model is frequently used in studying four wave mixing in a two-level medium, squeezing, etc. [19–21], and lately also has been used for the study of cone emission by many groups [13,15–18]. We find that due to the nonlinear saturation caused by the driving of the coherent component of the field, spectral regions with significant gain exist close to the resonance. The consequent evolution of the spectrum of the propagating field displays interesting features and in the stationary limit, a broadening of the spectral line always eventually happens, which is in contradiction to the coherent narrowing phenomena for pulsed propagation [1–4]. It may shed some new light on the mechanisms of cone emission.

The paper is organized as follows. In Sec. II we formulate and briefly review the approximations leading to the Langevin operator equations for the system. In Sec. III we point out an additional decorrelation that is involved in obtaining the semiclassical Maxwell-Bloch equation. In Sec. IV we discuss the results of our comparative numerical studies of the linearization approximation. We conclude in Sec. V.

II. FORMULATION

Our model system consists of a one-way propagating laser field that is tuned near resonance with a dense gaseous medium of two-level atoms. The Langevin operator equations that describe the propagation take the form

$$\begin{aligned}
&\left(\frac{\partial}{\partial z}+i\frac{1}{2k_L}\nabla_\perp^2\right)\hat{\Omega}^+(\vec{r},\tau)=i\frac{3\pi}{k_L^2}\gamma_{21}\mathcal{N}(\vec{r})\hat{\sigma}_+(\vec{r},\tau),\\
&\frac{\partial}{\partial\tau}\hat{\sigma}_+(\vec{r},\tau)=-\left(\frac{\gamma_{21}}{2}+\gamma_{21}^c+i\delta_p\right)\hat{\sigma}_+-i\hat{\Omega}^+\hat{\sigma}_z+\hat{F}_+,\\
&\frac{\partial}{\partial\tau}\hat{\sigma}_z(\vec{r},\tau)=-\gamma_{21}\left(\frac{1}{2}+\hat{\sigma}_z\right)+i\frac{1}{2}(\hat{\Omega}^+\hat{\sigma}_--\hat{\sigma}_+\hat{\Omega}^-)+\hat{F}_z,\\
&\frac{\partial}{\partial\tau}\hat{\sigma}_-(\vec{r},\tau)=-\left(\frac{\gamma_{21}}{2}+\gamma_{21}^c-i\delta_p\right)\hat{\sigma}_-+i\hat{\sigma}_z\hat{\Omega}^-+\hat{F}_-.
\end{aligned}\tag{1}$$

Here $\hat{\Omega}^+$ ($\hat{\Omega}^-$) is the Rabi frequency of the positive (negative) frequency part of the propagating field. k_L is the center wave vector of the field. $\mathcal{N}(\vec{r})$ is the number density of the active two-level atoms. γ_{21} is the spontaneous

emission rate, while γ_{21}^c denote the collisional dephasing rate. $\delta_p = \omega_L - \omega_{eg}$ is the laser detuning. $\hat{\sigma}_\mu$ are collective atomic operators. $\hat{F}_\mu$ denote the Langevin noise terms. We treat all the atoms as fixed, thus neglecting the Doppler distribution.

A detailed derivation will not be given here as it can be found in many studies of similar problems [7–13]. However, a brief review of the commonly used approximations in obtaining the above equations are given below to help establish the problem.

Rotating wave approximation (RWA). The resonant character of the interaction (in the dipole form) allows us to make the RWA, which consists of transforming the system to the interaction picture with respect to electronic excitation (ω_{eg}) or due to coherent driving of the atoms by a laser (ω_L) and neglecting the rapidly oscillating (counterrotating) terms in the transformed Hamiltonian. This approximation relies on the huge difference between characteristic time scales of optical oscillations ($\sim 10^{14}$–10^{15} Hz) and other typical scales of the system (kHz–GHz), such as those related to collisional dephasings (γ_{21}^c), natural linewidth (γ_{21}), or Rabi frequencies due to the external driving field (Ω), etc.

Collective variable description. The Hamiltonian for the model can be easily written for (jth) atoms with the atomic distribution function $\delta(\vec{r} - \vec{r}^{(j)})$. However, in a complicated system involving so many atoms, the physics lies at the thermodynamic limit, which is macroscopic in nature. Effectively for the propagation problem, we would like to replace the paraxial field modes and the atomic coordinates by spatially localized paraxial fields (see the slowly varying amplitude approximation discussed below) and by macroscopic atomic densities and polarizations. We coarse grain the space into volume elements with dimensions $[\delta x, \delta y, \delta z]$ and the dimensionless atomic fields are defined according to

$$\hat{\sigma}_\mu(\vec{r}) = \sum_{j \in [\vec{r}; \delta x, \delta y, \delta z]} \hat{\sigma}_\mu^{(j)}. \tag{2}$$

In the continuum limit, they obey

$$[\hat{\sigma}_+(\vec{r}), \hat{\sigma}_-(\vec{r}')] = \frac{1}{\mathcal{N}(\vec{r})} 2\hat{\sigma}_z(\vec{r})\delta(\vec{r} - \vec{r}'),$$

$$[\hat{\sigma}_z(\vec{r}), \hat{\sigma}_\pm(\vec{r}')] = \pm \frac{1}{\mathcal{N}(\vec{r})} \hat{\sigma}_\pm(\vec{r})\delta(\vec{r} - \vec{r}'). \tag{3}$$

One-way propagation approximation. The one-way propagation approximation assumes that coherent counterpropagating fields will not be established in a self-consistent analysis. The atomic polarization as defined above in Eq. (2), involving a simple summation over the atoms inside a unit volume, is based on an independent-atom approach. When the medium density is high (more than one active atom per cubic wavelength), the difference between the applied and the local field can no longer be ignored. In classical electrodynamics, we get the so-called Lorentz-Lorenz relation relating the macroscopic field to the internal microscopic field that is actually experienced by the individual atom. We restrict the density to regimes where this correction is unimportant. The reason for a one-way propagational formulation is to avoid the complications due to feedback. However, if the self-field corrections are included, they represent a special kind of feedback [22]. The one-way propagational formulation is a result of the phase-matching requirements in the slowly varying envelope approximation. If spatial modulations or variations on the scale of a wavelength are present, reflected waves will be generated [23,24].

Slowly varying envelope approximation (SVEA). The slowly varying envelope approximation assumes that the variation of the field amplitude along the propagation direction is very slow over a wavelength; therefore the second-order derivatives along the propagation direction can be neglected in comparison with the first-order terms. Under the coarse graining approximation introduced above, the dimension of the spatial cell $(\delta V)^{\frac{1}{3}} = (\delta x \delta y \delta z)^{\frac{1}{3}}$ basically determines the resolution with which the system can be studied and also the dimensions of the Kronecker δ functions involved in Eq. (3). This dimension has a lower limit. It has to be larger than the radius of an atom if we are going to study macroscopic quantities, i.e., a_0, the Bohr radius. It also has an upper limit that can be obtained from the following consideration. The frequency widths in the Fourier space have to be large enough that frequency components within the Rabi sidebands can be correctly described. Therefore, along the propagation direction,

$$\Delta k_z \gg \sqrt{\Omega^2 + \delta_p^2}/c. \tag{4}$$

This results in

$$\delta z \ll c/\sqrt{\Omega^2 + \delta_p^2}, \tag{5}$$

which is consistent with the uncertainty principle and is also the criterion for the validity of the SVEA.

Comoving frame description. Depending on the preparation of the medium and also its geometry, the time variable t is not necessarily the most convenient natural choice for an independent variable. Our medium is assumed to have the shape of a pencil with the pump propagating along the axis. Under the approximation that the dispersion of the pump can be neglected [or otherwise included (see below)], we note that depending on the location of the atom along the axis, the natural choice of time is the retarded local time $\tau = t - z/c$ rather than t. It is with respect to the local time τ that the dynamics of the atoms located at different positions along the axis will be the same. This is a crucial point. For each individual atom the above choice is as good as any other choice. However, after we introduce the collective variable description Eq. (2), we have to deal with atomic operator field variables. In order to specify these field variable envelopes, we have to use a time that is the same for all the atoms. The linear dispersion of the nonresonant atom (background gas) will be neglected. By choosing $\tau = t - z/c$ [9,13,15] rather than $\tau = t - z/v(\omega)$ we are able to handle more than one spectral component and the nonlinear dispersion of the medium is accounted for via the polarization occurring on the right-hand side of the field equation.

III. DECORRELATION APPROXIMATION AND THE MAXWELL-BLOCH EQUATION

Physical observables can be obtained from quantum mechanical averages (expectation values) of the operators in Eq. (1). A direct quantum average $\langle\langle\ \rangle\rangle$ of Eq. (1) helps to make the transition to the semiclassical Maxwell-Bloch equation. This requires the introduction of yet another approximation that is usually overlooked. We term it a decorrelation approximation, which replaces the expectation values of the product of both field and atomic operators by the product of their respective expectation values according to

$$\langle\langle\hat{\Omega}^{\pm}(\vec{r},\tau)\hat{\sigma}_{\mu}(\vec{r},\tau)\rangle\rangle \longrightarrow \langle\langle\hat{\Omega}^{\pm}(\vec{r},\tau)\rangle\rangle\langle\langle\hat{\sigma}_{\mu}(\vec{r},\tau)\rangle\rangle. \tag{6}$$

This decorrelation approximation is not emphasized since it is equivalent to replacing the operators by c numbers in the product and subsequently ignoring the quantum noise. Making the following decomposition into c number parts $\langle\langle\ \rangle\rangle$ and quantum deviations $\delta\hat{\Omega}^{\pm}$ and $\delta\hat{\sigma}_{\mu}$, we have

$$\begin{aligned}\hat{\Omega}^{\pm}(\vec{r},\tau) &= \langle\langle\hat{\Omega}^{\pm}(\vec{r},\tau)\rangle\rangle + \delta\hat{\Omega}^{\pm}(\vec{r},\tau),\\ \hat{\sigma}_{\mu}(\vec{r},\tau) &= \langle\langle\hat{\sigma}_{\mu}(\vec{r},\tau)\rangle\rangle + \delta\hat{\sigma}_{\mu}(\vec{r},\tau).\end{aligned} \tag{7}$$

The substitution given by Eq. (6) into Eq. (1) neglects the three terms

$$\begin{aligned}&\delta\hat{\Omega}^{\pm}(\vec{r},\tau)\langle\langle\hat{\sigma}_{\mu}(\vec{r},\tau)\rangle\rangle,\\ &\langle\langle\hat{\Omega}^{\pm}(\vec{r},\tau)\rangle\rangle\delta\hat{\sigma}_{\mu}(\vec{r},\tau),\\ &\delta\hat{\Omega}^{\pm}(\vec{r},\tau)\delta\hat{\sigma}_{\mu}(\vec{r},\tau)\end{aligned} \tag{8}$$

that are responsible for the quantum noise in the Langevin operator equation Eq. (1). In this propagation study, where gain exists over a wide frequency region, the neglected quantum fluctuation terms as given in Eq. (8) are extremely important in the initiation stage, where the first term $\delta\hat{\Omega}^{\pm}(\vec{r},\tau)\langle\langle\hat{\sigma}_{\mu}(\vec{r},\tau)\rangle\rangle$ contributes directly to the gain of new frequency components, while the other two terms are also additional source terms for the field. To accommodate these new frequency component fields that are generated, usually as an *a priori* guess, one assumes that at the input face $z = 0$, in addition to the classical input field $\langle\langle\hat{\Omega}^{\pm}(\vec{r},\tau)\rangle\rangle_{z=0}$ some initial probe seeds exist at these new frequencies even though quantum mechanically $\langle\langle\delta\hat{\Omega}^{\pm}(\vec{r},\tau)\rangle\rangle_{z=0} = 0$. A consistent quantum mechanical treatment would require a master equation approach. The consequent analysis can be done in terms of Fokker-Planck equations and stochastic differential equations [11,12,17].

Despite all the approximations detailed above, semiclassical Maxwell-Bloch equations remain a useful tool for propagation problems: first, because the essential deterministic part of the interactions are well approximated, and quantum noise shows up only as perturbing terms scaled with the inverse number of atoms per discretized spatial cell. The initial noise can sometimes be approximated by semiclassical seed values for the otherwise fluctuating variables. Second, in many of the experiments, the laser spectra have significant wings (often due to ASE), which can be extremely broad, and the spectral density at the frequency of the so-called new frequency light components (close to the Rabi sidebands) can be a great deal larger than the spectral density of vacuum fluctuation (see estimates below). Therefore, at least in the Sr cone emission studies [25], what usually occurs experimentally is essentially an amplifier (from ASE) rather than the more interesting generator (from quantum noise). For simplicity, we make the subsitution by neglecting the c number quantum expectation value symbol $\langle\langle\ \rangle\rangle$ according to

$$\begin{aligned}\langle\langle\hat{\Omega}^{\pm}(\vec{r},\tau)\rangle\rangle &\longrightarrow \Omega^{\pm}(\vec{r},\tau),\\ \langle\langle\hat{\sigma}_{\mu}(\vec{r},\tau)\rangle\rangle &\longrightarrow \sigma_{\mu}(\vec{r},\tau),\end{aligned} \tag{9}$$

in the semiclassical Maxwell-Bloch equations obtained above. In the quasi-one-dimensional limit, they take the form

$$\begin{aligned}\frac{\partial}{\partial z}\Omega(z,\tau) &= i\frac{3\pi}{k_L^2}\gamma_{21}\mathcal{N}(\vec{r})\sigma_{+}(z,\tau),\\ \frac{\partial}{\partial\tau}\sigma_{+}(z,\tau) &= -\left(\frac{\gamma_{21}}{2}+\gamma_{21}^{c}+i\delta_{p}\right)\sigma_{+} - i\Omega\sigma_{z},\\ \frac{\partial}{\partial\tau}\sigma_{z}(z,\tau) &= -\gamma_{21}\left(\frac{1}{2}+\sigma_{z}\right) + i\frac{1}{2}(\Omega\sigma_{-} - \Omega^{*}\sigma_{+}).\end{aligned} \tag{10}$$

All the above variables are now classical c numbers and

$$\sigma_{-}(\vec{r},\tau) = [\sigma_{+}(\vec{r},\tau)]^{*}. \tag{11}$$

As explained above, a decorrelation approximation has been made that ignores the quantum fluctuations. Classical noise will be simulated by the introduction of a classical stochastic field at the input face. Therefore Eqs. (10) describe the semiclassical propagation dynamics of classical fluctuating c numbers (stochastic variables).

One famous family of solutions of the time-dependent coupled Maxwell-Bloch equation of the form Eq. (10) is related to the so-called optical area theorems [1]. In many of the experiments, pulsed lasers were used and typical spectral widths are much larger than both collisional and radiative widths. A time-dependent formulation is required to evaluate the spectral components of the light.

Our ultimate interest is in studying the stationary generation process for new frequencies of light, which are quantum in nature. In this study, we concentrate on the effects of the linearization approximation, which assumes that the generated sidebands are coherent. We use the semiclassical Maxwell-Bloch equations to give us insight into the validity of the linearization approximation by performing numerical simulations with the full set of equations as given in Eq. (10) and by performing numerical simulations with probe fields that have widths larger than γ_{21}. We compare the results of the full solutions with those obtained under the linearization approximation. In the $t \to \infty$ limit, the set of equations for the coherent amplitudes reduce to the steady state propagation of the coherent field part as given by Eq. (13) below. In steady state, the solution for the intensity of the field can be obtained analytically [26].

IV. EFFECT OF LINEARIZATION APPROXIMATION

Now we discuss the critical linearization approximation that is often used in studying Eq. (10). We will discuss the propagation of wideband ASE noise that is inherent in the output from realistic pulsed laser. Using the same decomposition as given in Eq. (7) (except now classical averages are involved)

$$\begin{aligned}\Omega(z,\tau) &= \langle\Omega(z,\tau)\rangle + \delta\Omega(z,\tau),\\ \sigma_\mu(z,\tau) &= \langle\sigma_\mu(z,\tau)\rangle + \delta\sigma_\mu(z,\tau),\end{aligned} \tag{12}$$

we arrive at the following sets of equations: for the coherent part

$$\begin{aligned}\frac{\partial}{\partial z}\langle\Omega(z,\tau)\rangle &= i\frac{3\pi}{k_L^2}\gamma_{21}\mathcal{N}(\vec{r})\langle\sigma_+(z,\tau)\rangle,\\ \frac{\partial}{\partial\tau}\langle\sigma_+(z,\tau)\rangle &= -\left(\frac{\gamma_{21}}{2}+\gamma_{21}^c+i\delta_p\right)\langle\sigma_+\rangle - i\langle\Omega\rangle\langle\sigma_z\rangle,\\ \frac{\partial}{\partial\tau}\langle\sigma_z(z,\tau)\rangle &= -\gamma_{21}\left(\frac{1}{2}+\langle\sigma_z\rangle\right)\\ &\quad +i\frac{1}{2}[\langle\Omega\rangle\langle\sigma_-\rangle - \langle\Omega^*\rangle\langle\sigma_+\rangle]\end{aligned} \tag{13}$$

and for the quantities giving the deviations from the coherent part

$$\begin{aligned}\frac{\partial}{\partial z}\delta\Omega(z,\tau) &= i\frac{3\pi}{k_L^2}\gamma_{21}\mathcal{N}(\vec{r})\delta\sigma_+(\vec{r},\tau),\\ \frac{\partial}{\partial\tau}\delta\sigma_+(z,\tau) &= -\left(\frac{\gamma_{21}}{2}+\gamma_{21}^c+i\delta_p\right)\delta\sigma_+\\ &\quad -i\langle\Omega\rangle\delta\sigma_z - i\delta\Omega\langle\sigma_z\rangle - \underline{i\delta\Omega\delta\sigma_z},\\ \frac{\partial}{\partial\tau}\delta\sigma_z(z,\tau) &= -\gamma_{21}\delta\sigma_z + i\frac{1}{2}[\langle\Omega\rangle\delta\sigma_- - \langle\Omega^*\rangle\delta\sigma_+]\\ &\quad +i\frac{1}{2}[\delta\Omega\langle\sigma_-\rangle - \delta\Omega^*\langle\sigma_+\rangle]\\ &\quad +i\frac{1}{2}[\underline{\delta\Omega\delta\sigma_- - \delta\Omega^*\delta\sigma_+}],\end{aligned} \tag{14}$$

where $\langle\,\rangle$ denotes the classical stochastic average over fluctuations responsible for the broadband width of the propagating field. In the time-dependent study, the solution of the above equations has certain advantages over the direct simulation of the Maxwell-Bloch equations Eq. (10), especially when the input fields have a small fluctuating component. With the above decomposition, the deterministic large coherent amplitude can be solved to a much higher accuracy. Linearization corresponds to neglecting the underlined terms, which are quadratic in the variations. The physics of the linearization is based on the belief that any weak probe will not generate new sidebands of significant magnitudes.

In a linearized study, one often assumes a monochromatic time variation for the $\langle\delta\Omega^{\pm}(z,\tau)\rangle$ in order to solve for the polarizations at the sidebands in terms of the fields and consequently obtain closed coupled equations for field components only. In general the $\langle\delta\Omega^{\pm}(z,\tau)\rangle$ fluctuates on a time scale at least of order $1/\gamma_{21}$, so this monochromatic variation can only be considered valid in some "average over a bandwidth" sense. In this semiclassical study, we assume that the initial input probe field (the required seed) can be represented by a chaotic field model to simulate the inherent ASE in the pump field in the region of interest around the new frequency component. Such a chaotic field approximates the output of a multimode laser. It is assumed that [27]

$$\delta\Omega(z=0,t) = e^{-i\omega_L t}[\Omega_b(t)e^{i\omega_s t - i\varphi(0)}], \tag{15}$$

with

$$\Omega_b(t) = \Omega_{b0}\left[\zeta_R(t)+\zeta_I(t)\right], \tag{16}$$

where $\zeta_\mu(t)$ are real Wiener processes satisfying

$$\begin{aligned}\langle\zeta_\mu(t)\rangle &= 0,\\ \langle\zeta_\mu(t)\zeta_{\mu'}(t')\rangle &= \delta_{\mu\mu'}\frac{1}{2}e^{-\gamma_b|t-t'|}.\end{aligned} \tag{17}$$

The probe field spectrum at the input face of the cell is therefore

$$\begin{aligned}P_E(z=0,\omega) &= \int_{-\infty}^{\infty}\langle\Omega_b(0,t)\Omega_b^*(0,t+t')\rangle e^{-i\omega t'}dt'\\ &= |\Omega_{b0}^2|\frac{2\gamma_b}{(\omega-\omega_s)^2+\gamma_b^2}\end{aligned} \tag{18}$$

with a full width at half maximum given by γ_b. The ζ's can be obtained from integrating the Ito SDE [28]

$$d\zeta = -\gamma_b\zeta dt + \sqrt{\gamma_b}dW. \tag{19}$$

In the simulations we present, the initial phase $\varphi(0)$ was assumed to be a uniform random variable $\in[0,2\pi)$. Such a procedure enforces the fact that the probe field Ω_b and the coherent pump field are derived from completely uncorrelated sources.

The parameters used correspond to the Sr system with $\gamma_{21} = (2\pi)\,32.5$ MHz and a resonant broadening coefficient $\sim 14\mathcal{N}$ MHz, where the density $\mathcal{N}$ is in units of 10^{14} cm^{-3}. The pump laser of power 80 kW corresponding to the peak power of our laser pulse of a width ~ 1 ns gives a Rabi frequency of ~ 64 GHz. In order to simulate the spectral width between Rabi sidebands, an extremely small time step is required in accordance with the Heisenberg uncertainty principle. In this model study, we decided to use a Rabi frequency $\Omega = 4$ GHz at the input face $z = 0$, keeping $\delta_p = 2$ GHz, thus approximately keeping the ratio between these quantities the same as in the self-trapped filaments of the experimental situation. The colored sideband probe field is centered at the exact lower Rabi sideband position of the atom due to the input plane pump field alone. The density $\mathcal{N}$ is taken to be 2.5×10^{13} cm^{-3} unless otherwise specified, much smaller than in the actual experiments, as Doppler averaging is not included (the Doppler width is ~ 3 GHz). After first propagating the system into the stationary regime, the simulation for the spectrum involves taking successive points (2048) in the time series. The waiting time between sampling windows is 5 times the lifetime of the excited state. Total propagation distance is 1 cm.

The stationary spectrum is defined as

$$I(\omega-\omega_L)=\langle\Omega(\omega)\Omega^*(\omega)\rangle=\left\langle\left|\frac{1}{2T_0}\int_{-T_0}^{T_0}e^{-i\omega t}\Omega(t)dt\right|^2\right\rangle$$
$$=|\langle\Omega\rangle|^2\mathrm{sinc}^2(\omega T_0)+2\mathrm{Re}\left(\langle\Omega\rangle\mathrm{sinc}(\omega T_0)\frac{1}{2T_0}\int_{-T_0}^{T_0}e^{i\omega t}\langle\delta\Omega^*(t)\rangle dt\right)+\left\langle\left|\frac{1}{2T_0}\int_{-T_0}^{T_0}e^{-i\omega t}\delta\Omega(t)dt\right|^2\right\rangle, \quad (20)$$

where $\mathrm{Re}(x)$ represents the real part of x and the spectral function due to limited time window is

$$\mathrm{sinc}(x)=\frac{\sin(x)}{x} \quad (21)$$

where $2T_0$ is the sampling time and the spectral resolution $1/2T_0$ is of the order of one spontaneous decay rate. In the limit $T_0\to\infty$, or in the limit of discretized Fourier transformation, the above spectral function goes to $\delta(\omega-\omega_L)$. We can see that due to new frequency generation in the subsequent propagation (semiclassical), the variations $\delta\Omega(t)$ could have a nonzero average and would give a "coherent" component $\langle\delta\Omega(t)\rangle$ at that frequency even with a zero input.

In this semiclassical study, we have to give an initial probe amplitude as well. The spontaneous emission reservoir is considered to be at zero temperature, therefore the normal ordered intensity is zero. However, the study of quantum initiation in superfluorescence has indicated that in the linear regime, the antinormal ordered intensity for the paraxial modes can be considered as a proper probe field source [7,8,10]. It is interesting to make estimates here about the strength of the paraxial vacuum fluctuations (variance). The paraxial vacuum field expressed in terms of the standard mode expansion is [7–10]

$$\hat{\Omega}^{\pm}_{\mathrm{vac}}(\vec{r},t)=\mp i\sum_{\lambda\in\mathrm{paraxial}}g_\lambda e^{\mp i\vec{k}_\lambda\cdot\vec{r}}\hat{a}^{\pm}_\lambda, \quad (22)$$

with the creation (annihilation) operator $\hat{a}^+_\lambda$ ($\hat{a}^-_\lambda$) for the mode λ. The Rabi frequency for one mode is

$$g_\lambda=\sqrt{\frac{2\pi\hbar\omega_\lambda}{V}}\vec{\epsilon}\cdot\vec{d}/\hbar. \quad (23)$$

The antinormal ordered paraxial vacuum intensity is

$$I_{\mathrm{vac}}(\vec{r},t)=\langle\hat{\Omega}^-_{\mathrm{vac}}(\vec{r},t)\hat{\Omega}^+_{\mathrm{vac}}(\vec{r},t)\rangle$$
$$=\sum_{\lambda\in\mathrm{paraxial}}|g_\lambda|^2, \quad (24)$$

which would be divergent if integration over λ were not restricted to paraxial modes only.

In a quasi-one-dimensional model for the propagation, only those modes with $\vec{k}_\lambda$ pointing in the propagation direction can be considered to contribute to the initiation seed. The solid angle $d\Omega$ associated with these modes depends on the Fresnel number of the system. For an active volume $V=\pi R^2Z$, with $R=1$ mm and $Z=1$ cm for the Sr transition dipole moment d ($\gamma_{21}\sim 32.5$ MHz), we have $g_\lambda\sim 35$ kHz $\ll\gamma_{21}$. With the same parameters, an effective solid angle can be calculated according to

$$d\Omega=\pi R^2/Z^2\approx\pi\times 10^{-2}. \quad (25)$$

If we consider only modes of the vacuum within this solid angle of $\pi\times 10^{-2}$ and assume a bandwidth of the order of 100 GHz (chosen to represent the bandwidth of the observed cone emission), the intensity given by Eq. (24) corresponds to a Rabi frequency ~ 2.5 MHz, which is also much less than the spontaneous emission rate γ_{21}. The equivalent total power within this huge bandwidth is only of order of 30 μW cm^{-2}. In practice, the important bandwidth of the vacuum field may be only a few γ_{21}, therefore, the effective Rabi frequency for the vacuum field can be of the order of $10^{-2}\gamma_{21}$ or less. In a realistic pulsed laser, if we require that a coherent output field corresponds to a Rabi frequency of ~ 2 GHz (corresponding to a power of ~ 80 W cm^{-2} for the Sr $5\,^1S$–$6\,^1P$ transition), an effective Rabi frequency of ~ 2.5 MHz from ASE within a 100 GHz bandwidth would be equivalent to a requirement of the total ASE power to be less than 10^{-6} of the total laser power (and if we had taken a bandwidth of γ_{21} this power would be $\sim 10^{-10}$ of the total laser power). This stringent requirement is therefore difficult to meet. We conclude that in most experiments with pulsed lasers, the initial ASE input at the new frequencies is going to be more important than the initiation due to vacuum fluctuations. To study the initiation of new frequency components from the vacuum, cw laser driven systems would be more appropriate. With well stabilized lasers, ASE can be apparently suppressed in the far wing to the shot noise (vacuum fluctuation) levels discussed above [29]. We note, however, that the calculations with ASE input are only appropriate for a semiclassical study.

In this model study, we have used $\Omega^{\pm}_{s0}=0.4$ MHz, which is much smaller than the ASE present in the pulse. Therefore, the linear regime can be studied carefully.

We confirmed that the parametric gain due to four-wave mixing is the mechanism responsible for the growth of both sidebands [13–16]. However, due to the attenuation of the pump field, the gain region gradually moves in toward the coherent laser frequency as the Rabi frequency decreases. During the early stages of the propagation, the absorption of the lower frequency sideband is significant, which results in the splitting of each sideband into a doublet [15,16]. We have chosen the above parameters so that at the end of the propagation, the total power spectrum is still dominated by the coherent pump. In all simulations, we find no sign of spectral narrowing, as implied by conventional wisdom based on a gain argument. When the initial probe has a bandwidth much larger than the spontaneous emission rate, one of the absorption induced doublet components will gradu-

ally fade away due to absorption in further propagation. This may look like a narrowing; however, on further propagation, it eventually gets broader again. In the exact treatment without linearization, we found the mechanism for spectral broadening is initially through a sequence of generation of higher-order multiple sidebands. Though these higher-order sidebands are weak, their perturbation on the atoms is not. They drive the atoms in such a way that the emission can be changed from dominantly the first sideband emission to a broad spectral emission covering the region of many sidebands. Eventually, the higher-order sidebands merge into a broad background. Due to the same reason, the pump field also attains a broad feature with the width much larger than the spontaneous emission rate. Upon further propagation, all the structure disappears and all the power in the coherent pump gets redistributed into other frequencies. We are then left with a broadband output field. This picture is consistent with resonance fluorescence studies with more than one coherent component in the pump field [30,31]. The simulations indicate that the failure of the linearization is due to higher-order sidebands (or, equivalently, the saturation of the first-order sideband). This is also consistent with analytical model studies of sideband saturation with monochromatic sidebands [32]. We have also conducted an independent set of calculations with the same parameters, with a linearization achieved by neglecting quadratic underlined terms in Eq. (14). We found that, as expected, the two sidebands were simply amplified by the parametric gain profile calculated to all orders in the pump field (and does not depend on the sideband field) [14–16]. This is in violation of total energy conservation. The two sideband simply kept growing with propagation at a steady rate and eventually became unphysical. However, even in this case, we did not find any evidence for the spectral narrowing to a width below the spontaneous emission rate within the propagation distance. Figure 1 is a surface plot of the dynamic evolution of the spectral density for the chaotic probe field with $\gamma_b = 3\gamma_{21}$. In order to show the details of the evolution, a logarithmic scale is used. Figure 2 corresponds to the result of the linearized calculation with the same set of parameters. We have shown the surface in the same range as that of Fig. 1; the flatter top near the end of propagation is a numerical cutoff effect as we kept the plotting range to be the same as in Fig. 1. As expected, after an initial region of absorptive propagation, the propagated spectral density merely reflects the parametric gain profile.

For clarity, successive cross sections from Fig. 1 are plotted in Fig. 3. Close to the input face, the spectrum is very close to the linearized calculations and the initial splitting of the sidebands is due to absorption at the line centers corresponding to transitions in the dressed atom. No spectral broadening is evidenced here. We can already see the secondary sidebands starting to appear in the last plot. The next two plots of Figs. 4 and 5 show in detail multiple sideband generation accompanied by the spectral broadening of the whole background.

In these simulations, the spectral resolution is $\sim 0.9\gamma_{21}$. Therefore, the sideband widths can only be determined to within a resolution of the order of γ_{21}. In practice, due to the limited sampling of only 100 averages, the spectral profiles also show small scale fluctuations consistent with the expectations from the central limit theorem. In almost all stages of the propagation, the line shape is far more complicated than a simple Gauss-

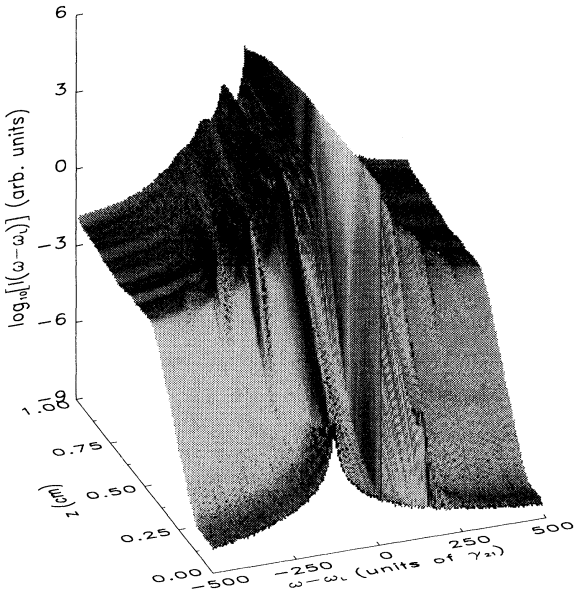

FIG. 1. Propagational evolution of the spectral density for a chaotic probe field input with a bandwidth $\gamma_b = 3$ (γ_{21}).

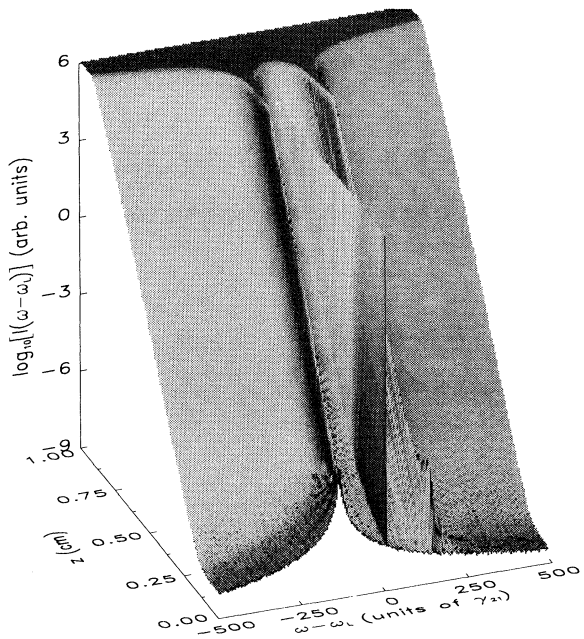

FIG. 2. Same as Fig. 1, except for the linearized case.

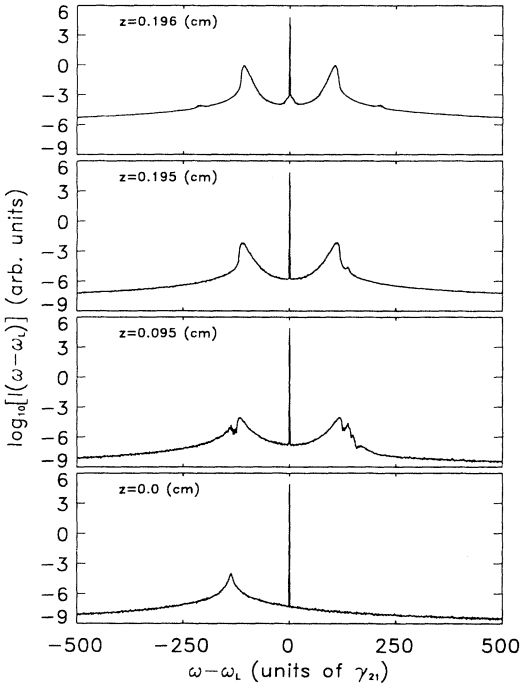

FIG. 3. Four cross sections from Fig. 1 at successive propagation distance z, as labeled in the figure.

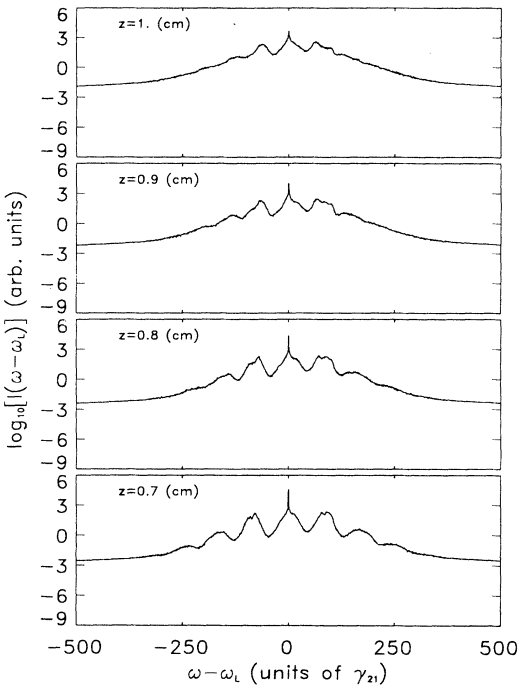

FIG. 5. Four cross sections from Fig. 1 in the nonlinear region at successive propagation distance z, as labeled in the figure. Overall spectral broadening and disappearance of the distinct sideband structures are shown.

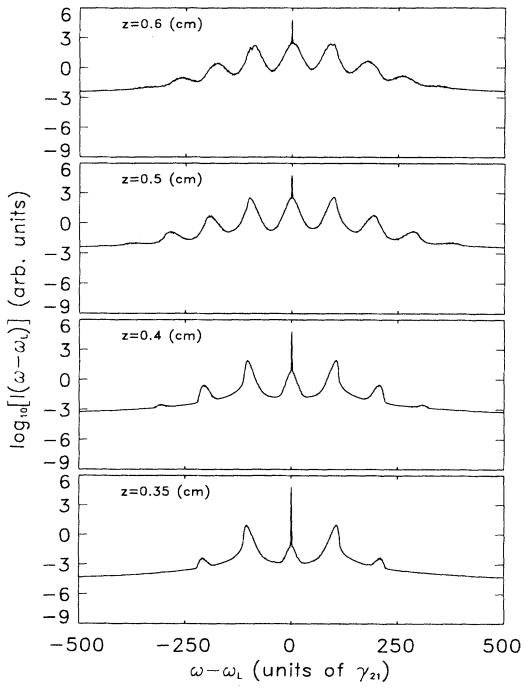

FIG. 4. Four cross sections from Fig. 1 in the nonlinear region at successive propagation distance z, as labeled in the figure. Multiple sideband generation is clearly shown.

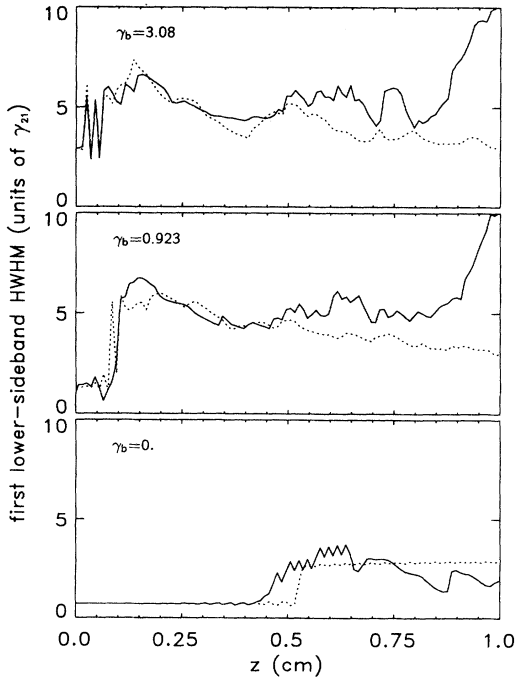

FIG. 6. Solid line denotes the full nonlinear calculations, while the dotted line represents the result from linearized theory. As denoted, each figure shows the result for $\gamma_b = 0$, 0.923, and 3.08 (γ_{21}), respectively.

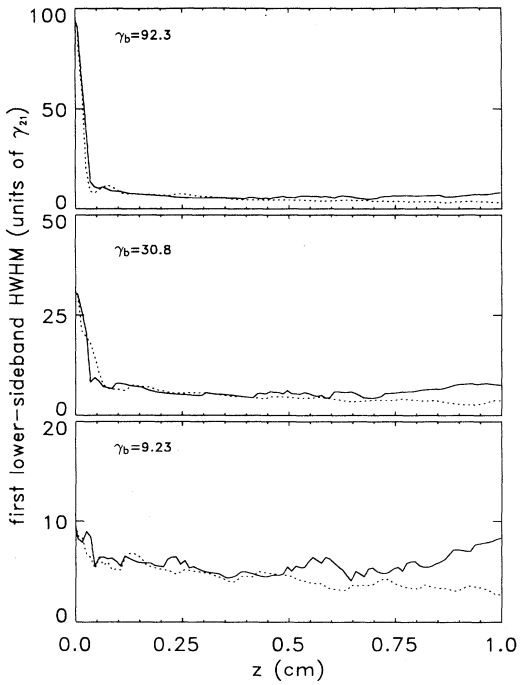

FIG. 7. Same as in Fig. 6, except now for $\gamma_b = 9.23$, 30.8, and 92.3 (γ_{21}), respectively.

ian or Lorentzian one. We decided to take the width of the sideband to be the standard half-width at half maximum irrespective of what kind of line shape it might possess. In the case when a distinct doublet is present, the width of the more intense component is used. If the doublet structure is overlapping significantly, the width of the whole structure is taken. We conclude that an average absolute accuracy of the order of γ_{21} is achieved for the width of a relatively narrow sideband, while an accuracy better than 10% is achieved for wide sidebands. In the following two plots, the first lower sideband width is plotted against propagation distance. In the first plot, Fig. 6, the clear trend of spectral broadening is obvious (note that $\gamma_b = 0$ corresponds to a coherent input whose phase is uncorrelated with the pump). The initial oscillations are due to the doublet formation within the sideband. In the second plot, Fig. 7, an overall spectral narrowing is shown in the early stage of propagation. Physically, this is due to absorption. The final width approaches a value much larger than the spontaneous emission rate γ_{21}. Upon further propagation, all the sidebands merge into one broad spectral feature centered at the laser frequency, the width of which is of the order of the Rabi frequency corresponding to the total power density in the field. We have also performed these simulations for a phase diffusion model [27,33] probe field with the same parameters as given above. Results do not show significant differences from those presented here for a chaotic probe field. Detailed comparisons will be given elsewhere.

V. CONCLUSIONS

We studied the effects of a linearization approximations often used in the propagational studies [14–16,19,20]. We found that in the stationary limit, wideband background noise due to either ASE or stochastic input can be amplified to appreciable levels through gain from the nonlinear coherent driving. Upon propagation into the medium, in the high optical density limit, the width of the background input does not experience any coherent narrowing as one might have guessed. If anything, the width becomes broader and the nonlinearity enhanced conversion from the monochromatic coherent component to other new frequency component results in a spectrally less pure field because ultimately this redistribution is caused through dissipative mechanisms associated with spontaneous emission as well as other dephasing mechanisms.

Within this semiclassical study, the conditions for the propagating field to be stationary can be understood by examining the coarse graining and the slowly varying envelope approximations and is further ensured operationally by monitoring the temporal evolution of the field during the spatial propagation. Equations (13) and (14) constitute a set of nonlinear equations for the propagating fields. At any spatial location, coarse grained atoms are driven by the forward propagating field (which is external to those atoms, but is already modified due to propagation up to this particular location by atoms up stream). The backward propagating (reflected) field is neglected under the slowly varying envelope approximation. Therefore the propagation nonlinearity acts only in one direction (along the propagation direction) without feedback. We expect that the neglect of backward propagating components will be valid at significantly low density of atomic vapor and with no significant spatial variations (which would give rise to reflected waves). Microscopically, the stationarity is a very complicated question, as the propagating field (which is the coarse grained field) results from the spatial averages from fields radiated by all the atoms. In practice, we find that for the parameters we are using, stationarity is achieved after the transients die away (on a time scale given by the inverse of the dissipative rate γ_{21}). After a certain number of sampling averages, the computed spectrum and the variance converge close to a final value and do not change significantly with a further increase of the ensemble size.

ACKNOWLEDGMENTS

We thank Dr. A. Gallagher, Dr. J. Guo, Dr. R. Hart, and Dr. M. Lewenstein for enlightening discussions. This work is supported in part by NSF Grant No. PHY90-12244 through the University of Colorado. The work of L.Y. is also supported by the National Science Foundation through a grant to the Institute for Theoretical Atomic and Molecular Physics at Harvard University and Smithsonian Astrophysical Observatory.

[1] L. Allen and J. H. Eberly, *Optical Resonance and Two-level Atoms* (Dover, New York, 1987).
[2] B. W. Shore, *The Theory of Coherent Atomic Excitation, I. Simple Atoms and Fields, II. Multilevel Atoms and Incoherence* (Wiley, New York, 1990).
[3] T. Von Foerster and R. J. Glauber, Phys. Rev. A **3**, 1484 (1971).
[4] L. N. Menegozzi and W. E. Lamb, Jr., Phys. Rev. A **17**, 701 (1978).
[5] E. L. Dawes and J. H. Marburger, Phys. Rev. **179**, 862 (1969).
[6] A. W. McCord, Ph.D. thesis, University of Otago, Dunedin, Zealand, 1988.
[7] D. Polder, M. F. H. Schuurmans, and Q. H. F. Vrehen, Phys. Rev. A **19**, 1192 (1979), and references therein.
[8] F. Haake, H. King, G. Schroder, J. Haus, and R. Glauber, Phys. Rev. A **20**, 2047 (1979).
[9] M. G. Raymer and J. Mostowski, Phys. Rev. A **24**, 1980 (1981).
[10] L. You, J. Cooper, and M. Trippenbach, J. Opt. Soc. Am. B **8**, 1139 (1991).
[11] R. Graham and H. Haken, Z. Phys. **213**, 420 (1968); **234**, 193 (1970); **235**, 166 (1970); **237**, 31 (1970).
[12] P. D. Drummond and M. G. Raymer, Phys. Rev. A **44**, 2072 (1991).
[13] L. You, J. Mostowski, and J. Cooper, Phys. Rev. A **46**, 2903 (1992); **46**, 2925 (1992).
[14] B. R. Mollow, Phys. Rev. A **7**, 1319 (1973).
[15] D. J. Harter, Ph.D. thesis, Institute of Optics, University of Rochester, 1982; D. J. Harter and R. W. Boyd, Phys. Rev. A **29**, 739 (1984).
[16] J. F. Valley, Ph.D. thesis, Optical Sciences Center, University of Arizona, 1989; J. F. Valley, G. Khitrova, H. M. Gibbs, J. W. Grantham, and Xu Jianjin, Phys. Rev. Lett. **64**, 2362 (1990).
[17] L. You, Ph.D. thesis, University of Colorado, 1993.
[18] W. Chalupczak, W. Gawlik, and J. Zachorowski, Phys. Rev. A **49**, 4895 (1994).
[19] M. D. Reid and D. F. Walls, Phys. Rev. A **34**, 4929 (1986); M. D. Reid, *ibid.* **37**, 4792 (1988).
[20] A series of papers based on this model were published by M. Sargent III *et al.*, the last one contains a listing, Phys. Rev. A **40**, 7039 (1989).
[21] M. E. Crenshaw and C. M. Bowden, Phys. Rev. Lett. **67**, 1226 (1991).
[22] J. P. Dowling and C. M. Bowden, Phys. Rev. Lett. **70**, 1421 (1993).
[23] B. R. Mollow, Phys. Rev. A **7**, 1319 (1973).
[24] R. Chang and P. Meystre, Phys. Rev. A **26**, 1510 (1991).
[25] R. Hart, L. You, A. Gallagher, and J. Cooper, Opt. Commun. **111**, 331 (1994).
[26] A. Icsevgi and W. E. Lamb, Jr., Phys. Rev. **185**, 517 (1969).
[27] M. H. Anderson, Ph.D. thesis, University of Colorado, 1992.
[28] C. W. Gardiner, *Quantum Noise* (Springer, Berlin, 1991).
[29] C. Oates (private communication); J. L. Hall and T. W. Hansch, Opt. Lett. **9**, 502 (1984).
[30] Y. Pomeau, B. Dorizzi, and B. Grammaticos, Phys. Rev. Lett. **56**, 681 (1986).
[31] M. Wilkens and K. Rzazewski, Phys. Rev. A **40**, 3164 (1989).
[32] Sunghyuck An and M. Sargent III, Phys. Rev. A **40**, 795 (1989).
[33] D. S. Elliott and S. J. Smith, J. Opt. Soc. Am. B **5**, 1927 (1988).

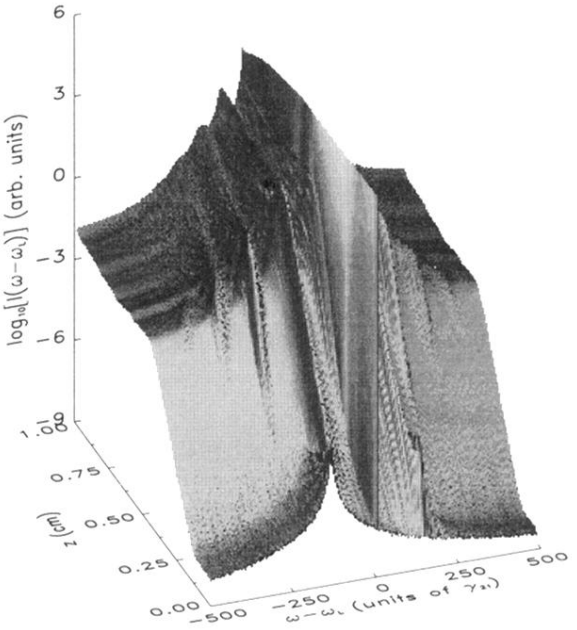

FIG. 1. Propagational evolution of the spectral density for a chaotic probe field input with a bandwidth $\gamma_b = 3$ (γ_{21}).

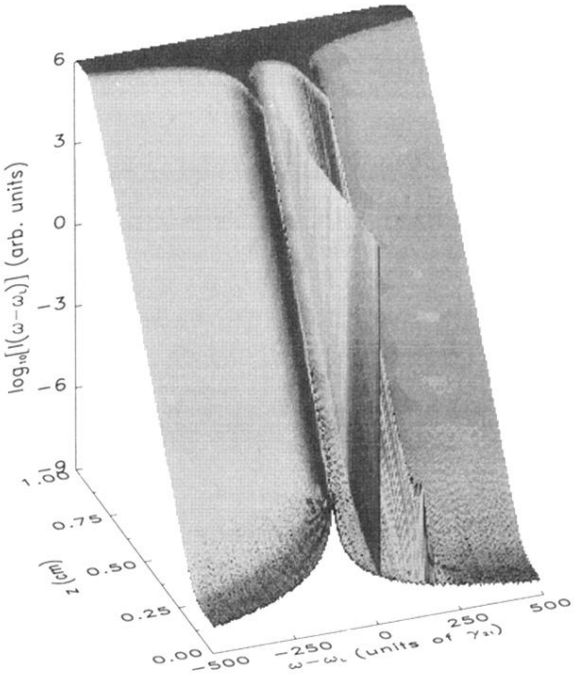

FIG. 2. Same as Fig. 1, except for the linearized case.